$CH(A^2\Delta)$ Formation in Hydrocarbon Combustion: The Temperature Dependence of the Rate Constant of the Reaction $C_2H + O_2 \rightarrow CH(A^2\Delta) + CO_2$

Rehab M. I. Elsamra, Stijn Vranckx, and Shaun A. Carl*

University of Leuven, Department of Chemistry, Celestijnenlaan 200F, Leuven, Belgium

Received: July 6, 2005; In Final Form: August 26, 2005

The temperature dependence of the rate constant of the chemiluminescence reaction $C_2H + O_2 \rightarrow CH(A) + CO_2$, k_{1e}, has been experimentally determined over the temperature range 316−837 K using pulsed laser photolysis techniques. The rate constant was found to have a pronounced positive temperature dependence given by $k_{1e}(T) = AT^{4.4} \exp(1150 \pm 150/T)$, where $A = 1 \times 10^{-27}$ cm^3 s^{-1}. The preexponential factor for k_{1e}, A, which is known only to within an order of magnitude, is based on a revised expression for the rate constant for the $C_2H + O(^3P) \rightarrow CH(A) + CO$ reaction, k_{2b}, of $(1.0 \pm 0.5) \times 10^{-11} \exp(-230\ K/T)$ cm^3 s^{-1} [Devriendt, K.; Van Look, H.; Ceursters, B.; Peeters, J. *Chem. Phys. Lett.* **1996**, *261*, 450] and a k_{2b}/k_{1e} determination of this work of 1200 ± 500 at 295 K. Using the temperature dependence of the rate constant $k_{1e}(T)/k_{1e}(300\ K)$, which is much more accurately and precisely determined than is A, we predict an increase in k_{1e} of a factor 60 ± 16 between 300 and 1500 K. The ratio of rate constants k_{2b}/k_{1e} is predicted to change from 1200 ± 500 at 295 K to 40 ± 25 at 1500 K. These results suggest that the reaction $C_2H + O_2 \rightarrow CH(A) + CO_2$ contributes significantly to CH(A→X) chemiluminescence in hot flames and especially under fuel-lean conditions where it probably dominates the reaction $C_2H + O(^3P) \rightarrow CH(A) + CO$.

Introduction

In the absence of heated soot particles, having a continuum emission perceived as orange-yellow, hydrocarbon flames would be invisible were it not for the handful of electronically excited species with electronic transitions in the 150−300 kJ mol^{-1} range and superthermal populations. Most of these species have long been identified spectroscopically, CH($A^2\Delta$, $B^2\Sigma^-$), C_2($d^3\Pi_g$), CN($B^2\Sigma^+$), HCO($\tilde{A}^2A''$, $\tilde{B}^2A'$), CO($a'^3\Sigma$, $d^3\Delta$, $e^3\Sigma$), and $CO_2(\tilde{A}^1B_2)$,[1−7] and from their non-Boltzmann concentrations one must conclude their source to be either chemical reaction or rovibronic-to-rovibronic (E, $v, j \rightarrow E', v', j'$) energy transfer.[8] However, finding the reactions responsible for their production and determining the associated rate constants have proven to be difficult challenges.

Quantitative interpretation of flame chemiluminescence data, in terms of the concentration of one of the precursor species or the precursor concentration product, requires some knowledge of the magnitude of the rate constant. Unfortunately though, despite several attempts at their determination, accurate absolute rate constants have not been forthcoming for the gas-phase chemiluminescence reactions. This is due simply to the combined uncertainties associated with the determination of absolute concentrations of both (mainly radical) precursors and the electronically excited product. Thus, absolute rate constants determined so far for these reactions are probably known only within about an order of magnitude. Nevertheless, attempts to interpret flame chemiluminescence go back many years, with much recent work focusing on qualitatively linking OH(A→X) and CH(A→X) emission intensities[9] to flame equivalence ratios[10,11−13] heat release rates,[14,15] and the final stages of the C_2-hydrocarbon and CH_x reaction chains.[16,17]

In this paper we focus on the chemical reactions responsible for the production of $CH(A^2\Delta)$ and, by extension, $CH(B^2\Sigma^-)$. The former gives rise to the relatively intense blue emission at ca. 430 nm, and the latter to a less intense emission, just beyond the visible range, at ca. 390 nm. The transition at 430 nm can be readily observed in natural gas flames by the unaided eye.

Only a few reactions stand out as being plausible sources of electronically exited CH in flame environments. Of these, only

		$\Delta_r H_{298K}$/kJ mol^{-1}	
$C_2H + O_2$	→ CH(B, A) + CO_2	−56, −85	(R1c,e)
$C_2H + O$	→ CH(B, A) + CO	−22, −51	(R2a,b)
C + H + M	→ CH(B, A) + M	−24, −53	(R3a,b)
C_2 + OH	→ CH(C, B, A) + CO	−1.5, −74, −103	(R4a,b,c)
$C_2 + HO_2$	→ OH(A) + C_2O	−36	(R5a)
	→ CH(C, B, A) + CO_2	−262, −335, −364	(R5b,c,d)
$C_2 + NH_2$	→ CH(B, A) + HCN	+19, −10	(R6a,b)
$C_2 + CH_3O$	→ CH(A) + H_2CCO	−21	(R7)
CH + HONC	→ CH(B, A) + HNCO	−15, −44	(R8a,b)
CH + HCNO	→ CH(A) + HNCO	−3	(R9a)
HOCC + O	→ CH(B, A) + CO_2	−29, −58	(R10a,b)

studies of R1, R2, and R4 have so far appeared in the literature: for the other reactions, the overall rate constants and yield of electronically excited CH is unknown. However, it has become clear over recent years that most, if not all, CH(A) formed in hydrocarbon flames is associated with the simultaneous presence of C_2H_2 and O (and therefore usually O_2). Reaction R2b was proposed many years ago by Glass et al.[18] as being the main source of CH(A) in ethyne and methane flames. The other main contenders for CH(A) formation have been the C_2 + OH reaction (R4c) proposed by Gaydon[19] and by Porter et al.[20] and reaction R1e proposed by Matsuda et al.[21] and by Renlund et al.[22]

For R1 and R2, the combination of the high C−H bond strength of C_2H and a very stable coproduct leads to sufficient

* Corresponding author. E-mail: shaun.carl@chem.kuleuven.be.

10.1021/jp053684b CCC: $30.25
Published on Web 10/20/2005

excess energy available for electronic excitation of CH and, for R1, also of HCO. Further support for the plausibility of these

		$\Delta_r H_{298K}$/kJ mol^{-1}	
$C_2H + O_2 \rightarrow$	HOCC + O	−26	(1a)
	H + C + CO_2	−32	(1b)
	CH($B^2\Sigma^-$) + CO_2	−56	(1c)
	COOH + C	−76	(1d)
	CH($A^2\Delta$) + CO_2	−85	(1e)
	HCCO + O	−140	(1f)
	$C_2O(\tilde{X}^3\Sigma^-,\tilde{a}^1\Delta, \tilde{b}^1\Sigma^+)$ + OH	−145, −73, −40	(1g)
	CH($a^4\Sigma^-$) + CO_2	−291	(1h)
	CH + CO_2	−362	(1i)
	H + CO + CO	−568	(1j)
	$HCO(\tilde{X}^2A', \tilde{A}^2A''(\Pi), \tilde{B}^2A')$ + CO	−634, −523, −173	(1k)

		$\Delta_r H_{298K}$/kJ mol^{-1}	
$C_2H + O(^3P) \rightarrow$	CH($B^2\Sigma^-$) + CO	−22	(2a)
	CH($A^2\Delta$) + CO	−51	(2b)
	HCO + C	−63	(2c)
	CH($a^4\Sigma^-$) + CO	−257	(2e)
	H + $C_2O(\tilde{X}^3\Sigma^-,\tilde{a}^1\Delta, \tilde{b}^1\Sigma^+)$	−309, −142, −109	(2d)
	CH + CO	−328	(2f)
	HOCC	−524	(2g)
	HCCO	−638	(2h)

two reactions is provided by the work of Peeters and coworkers,[23−26] who showed C_2H radicals to be efficiently generated, even at low temperatures, after several fast reactions following the oxidation of C_2H_2 by O. This low-temperature mechanism also probably explains the blue emission observed when ethyne is released in the upper atmosphere, given that the multireaction sequence involves only C_2H_2 and O as coreactants. For this reason, CH(A) emission might also be observed in regions of planetary atmospheres, such as Saturn's, having significant mole fractions C_2H_2 and O atoms.[26]

By demonstrating the proportionality of the CH(A→X) emission intensity to the product $[C_2H][O]$, Devriendt and Peeters[27] showed reaction R2b to be a major source of CH(A) in low-pressure C_2H_2/O/H atomic flames. In the same study the absolute rate constant for R2b over the temperature range 290−925 K was determined as $k_{2b} = 2.46 \times 10^{-11} \exp(-230\ K/T)$. However, in consideration of a single-temperature determination by the same group and more recent quantum yield data for the $C_2H_2 + h\nu(193\ nm) \rightarrow C_2H + H$, we consider the best Arrhenius expression for this reaction to be $k_{2b} = (1.0 \pm 0.5) \times 10^{-11} \exp(-230\ K/T)\ cm^3\ s^{-1}$.[28] This represents an overall branching of R2 to R2b of about 10%.

Recently, Chikan et al.[29] reported a much higher branching to channel R2b of 60%, based on measurement of nascent excited vibrational distributions of CO and reliance on linear surprisal extrapolation to obtain CO(v=0) populations. However, these authors were in fact reporting the fraction [CH(A)]/([CH(X)] + [CH(A)]) and assumed that CH is produced in all reaction channels. However, a major fraction of the initial chemically activated HCCO is expected to dissociate to H + C_2O (triplet or singlet). The work of Devriendt et al.[28] and Chikan et al.[29] are in accord if the C_2O + H channel(s) account for ca. 80 ± 15% of the reaction.

The $C_2H + O_2$ reaction, proposed by Matsuda et al.,[21] is also known to yield CH(A).[22] Indeed, this reaction is routinely employed for the time-resolved monitoring of C_2H radicals in kinetic experiments[30−32] whereas, more recently, reaction R2b has also been employed for this purpose.[33] Comparison of these two techniques using the same experimental setup clearly shows the rate constant k_{2b} to be orders of magnitude greater than k_{1e} at room temperature. This observation was quantified by Devriendt et al.[28] who determined k_{2b}/k_{1e} at 290 K to be 500 ± 70 (not including the systematic uncertainty) by comparing the initial emission intensities at 430 nm following the photolysis of C_2H_2/O_2/He and C_2H_2/N_2O/He mixtures of known composition at 193 nm. Smith et al.[34] recently attempted to determine the rate constant for the formation reactions for CH(A) in low-pressure methane/air flames by measuring absolute CH(A) concentrations and fitting these to a kinetic model. These authors were not able though to clearly distinguish between R1e and R2b as the main source of CH(A) in their experiments.

Without then any clear data on the temperature dependence of the $C_2H + O_2 \rightarrow CH(A) + CO_2$ reaction, its role in flames is not certain. Should k_{1e} increase sharply with temperature, R1e could contribute significantly to the observed CH(A →X) chemiluminescence. Thus, the aim of the present investigation is to better assess the contribution of reaction R1e to flame chemiluminescence by direct determination of its temperature dependence. Further, such experimental data on chemiluminescence reactions can aid refinement of theoretical reaction dynamical models for elementary processes, especially with respect to nonadiabatic processes.[35]

Experimental Section

The experimental methodology for these measurements is quite straightforward. If C_2H is generated in the presence of excess O_2, CH(A) is formed, which rapidly reaches a quasi-steady-state concentration such that a chemiluminescence decay profile is observed having an intensity proportional to the product $[O_2][C_2H]$ and therefore a decay rate equal to the decay rate of $[C_2H]$. At time = 0 the emission intensity is well defined because $[C_2H]$ has not been diminished by reaction. If the temperature of the reaction vessel is changed, the intensities of the chemiluminescence profiles at time = 0 reflect changes in the initial densities of O_2 and C_2H with temperature (which are easily defined) as well as changes with temperature of the rate constant for the process $C_2H + O_2 \rightarrow CH(A) + CO_2$: the parameter required. Four further considerations for precise determination of $k_{1e}(T)/k_{1e}(T_{ref})$, which are explained in detail below are (i) quenching of CH(A) by N_2, (ii) the time required by CH(A) to reach quasi steady state, (iii) chemical generation of O-atoms, and (iv) changes in the fraction of photons passing though the interference filter.

The experimental setup used here is almost identical to that described for our recent study of the $C_2H + NO_2$ reaction.[33] The main points are briefly repeated here.

C_2H radicals were produced in a small tubular region along the center of a heatable stainless steel reaction cell by pulsed (8 Hz, 10 ns) 193 nm photolysis of ca. $(0.2-1.4) \times 10^{15}$ cm^{-3} C_2H_2, derived from a certified, acetone-free, mixture of C_2H_2 in high-purity He, in the presence of excess concentrations (ca. $0.2-5.6 \times 10^{15}$ cm^{-3}) of O_2 and 9−10 Torr nitrogen (99.995% purity).

$$C_2H_2 + h\nu\ (193\ nm) \rightarrow C_2H + H \qquad (R11)$$

Following its production, C_2H is removed, with a half-life of tens of microseconds, by reaction with constant concentrations of C_2H_2 and O_2

$$C_2H + C_2H_2 \rightarrow \text{products} \qquad (R12)$$

and therefore has a simple time dependence, given by

$$[C_2H]_t = [C_2H]_{t=0} \exp\{-(k_1[O_2] + k_{12}[C_2H_2])t\} \qquad (i)$$

The concentration of CH(A), produced via channel (R1e), effectively reaches quasi steady state within about 2 μs, i.e., about four CH(A→X) lifetimes. At any given temperature

$$\frac{d[CH(A)]_{ss}}{dt} = k_{1e}[C_2H][O_2] - k_{em}[CH(A)]_{ss} - k_{qN_2}[N_2][CH(A)]_{ss} = 0 \quad \text{(ii)}$$

such that, after this time, $[CH(A)]_{ss} \propto [C_2H]_t$. The collision-free radiative lifetime, $1/k_{em}$, of CH(A) is 540 ns.[36] Under our experimental conditions, nonradiative removal by collisions with C_2H_2 and O_2 is insignificant. Quenching by N_2 though needs to be taken into account. Although the rate constant for quenching by N_2, k_{qN_2}, is relatively small at room temperature, the process has an activation energy[37] and thus may be significant at higher temperatures. For this reason a direct determination of the CH(A) lifetime in the presence of 10 Torr N_2 as a function of temperature was carried out. N_2 was chosen as the buffer gas in these experiments over He (which has a negligible CH(A) collisional quenching rate at 10 Torr) to ensure a very rapid removal of any nonthermal electronic and/or vibrational energy of the nascent C_2H photoproducts.

As a function of time, and for a given temperature, the resulting CH(A→X) emission intensity from the center of the reactor, which is imaged onto an optically filtered (430 ± 10 nm, Oriel 59295) photomultiplier tube (R928, Hamamatsu), is given by

$$Iem_t = \Phi k_{em}[CH(A)]_{ss} = \frac{\Phi k_{em} k_{1e}[O_2][C_2H]_t}{k_{em} + k_{qN_2}[N_2]} \quad \text{(iii)}$$

and, at time = 0,

$$Iem_{t=0} = \frac{\Phi k_{em} k_{1e}[O_2][C_2H]_{t=0}}{k_{em} + k_{qN_2}[N_2]} \quad \text{(iv)}$$

where Φ represents the overall emitted-photons-to-voltage conversion efficiency of the detection system. Under our experimental conditions (10 Torr N_2) Φ is a weak function of temperature because the fraction of photons passing through the relatively narrow interference filter changes as the thermalized population of CH(A) rotational levels become broader with increasing temperature. This effect is taken into account by simulating the CH(A→X) emission envelope as a function of temperature and then calculating the change with temperature in the fraction of photons passing through the interference filter, relative to that at 320 K.

As mentioned earlier, to determine the temperature dependence of k_{1e}, one needs to determine the $t = 0$ intercept values of Iem (eq iv) as a function of temperature under conditions in which other parameters of eq iv remain either constant with temperature or have a well-characterized T dependence. A least-squares fit to the decay profile is used to precisely determine the $t = 0$ intensity value, rather than relying on a single measured point close to $t = 0$ (bearing in mind the ca. 2 μs approach to quasi steady state and removal over ca. 4 μs of any excess vibrational and rotational energy of nascent C_2H). Strictly, the emission intensity Iem profile always lags behind $[C_2H]_t$ by the average lifetime of CH(A), given by $[k_{em} + k_{qN_2}(T)[N_2](T)]^{-1}$. This would result in $t = 0$ intercept values being overestimated more for the faster decays observed at low temperatures than for the slower decays at high temperatures. To ensure that all decays were treated equally in this respect, the function $A \exp(-k'(t - \theta))$, where θ represents the lifetime of CH(A) at a given temperature, was fitted to each decay. This gives then $Iem_{t=\theta}$ rather than $Iem_{t=0}$. Using the latter would result in a ca. 7% relative error between the low- and high-temperature intercept determinations.

In the present experiments, the flows of O_2, C_2H_2, and carrier gas, as well as total pressure, were maintained constant as the temperature of the reaction zone was varied, so that the concentration product $[C_2H_2][O_2]$ at any temperature is easily related to the same product at a reference temperature, T_{ref}, by

$$[C_2H_2](T)\,[O_2](T) = [C_2H_2](T_{ref})\,[O_2](T_{ref})\,\{T_{ref}/T\}^2 \quad \text{(v)}$$

In this case, the overall temperature dependence of the intercept $Iem_{t=\theta}$, which is derived from least-squares fitting of the chemiluminescence decay profiles for $t > 5$ μs, is given by

$$\frac{k_{1e}(T)}{k_{1e}(T_{ref})} = \frac{Iem_{t=\theta}(T)}{Iem_{t=\theta}(T_{ref})}\left(\frac{T}{T_{ref}}\right)^2\left(\frac{\Phi(T_{ref})}{\Phi(T)}\right)\left\{\frac{k_{em} + k_{qN_2}(T)[N_2](T)}{k_{em} + k_{qN_2}(T_{ref})[N_2](T_{ref})}\right\} \quad \text{(vi)}$$

where the last quotient, representing the effects of CH(A) quenching by N_2, from hereon designated $Q(T)$, was determined in a separate experiment and compared to literature data.

$Iem_{t=\theta}$ values were determined over a temperature range 316−837 K for a range of conditions that differed in either flow rates (those of O_2, C_2H_2, or total flow) or photolysis pulse intensity or both. The temperature of the gas in the reaction region was measured using a cromel−alumel thermocouple situated 1 cm away from the path of the photolysis beam. We expect the uncertainty in temperature measurements to be ±3 K at 320 K and ±20 K at 830 K.

Each chemiluminescence intensity profile was constructed from two separate time profiles: the signal plus background and the background. The first was taken under normal conditions of C_2H_2, O_2, and N_2, and the second under identical conditions to the first but with N_2 substituted for O_2. The second profile, which is each time subtracted from the first, takes into account short-lived background emissions due to CH(A) produced by two-photon absorption of C_2H_2 at 193 nm, and any laser-induced silica-window fluorescence. Between 30 and 50 individual decays were averaged for each fitted emission profile.

Under certain conditions the T dependence of the integrated emission intensity, rather than the initial intensity, of the chemiluminescence profiles may be employed to extract the T dependence of k_{1e}. This requires that reaction of C_2H with O_2 (having a T-dependent rate constant) is only a small fraction of that due to reaction with C_2H_2 (having a T-independent rate constant) because then the C_2H removal rate may also be precisely defined as a function of temperature. For one set of experiments these conditions were met, with $k_{12}[C_2H_2]$ a factor of 13 greater than $k_1[O_2]$. Under these conditions the *integrated* emission intensity may be approximated by

$$\int_{t=0}^{t=\infty} Iem\, dt \propto \frac{k_{1e}(T)}{k_{12}(T)}\frac{[O_2]}{Q(T)} \propto \frac{k_{1e}(T)}{k_{12}(T)}\frac{\Phi(T)}{TQ(T)} \quad \text{(vii)}$$

which is independent of $[C_2H_2]$ because a change in $[C_2H_2]$ results then in an equal change in the C_2H production and removal rates. Thus $(G(T)\,Q(T)\,T)/\Phi(T)$, where G from hereon represents the integrated emission intensity, should be proportional to $k_{1e}(T)$, given that $k_{12}(T)$ is known to be independent of

temperature over the temperature range covered in these experiments.[38,39]

Based on recent potential-energy surface calculations of Sumathi et al.[40] and of Bai et al.[41] for R1, the predicted major product channels are R1k (→ HCO + CO) and R1f (→ HCCO + O). This requires that O(^{3}P) production and its possible interference be considered in our measurements because any O-atoms produced will react with C_2H to yield again CH(A), via R2b, having a much larger rate constant than R1e. For this reason, all of our experiments were performed using a 193 nm laser fluence of less than 10 mJ/cm^2 per pulse. Under typical conditions of 7×10^{14} cm^{-3} C_2H_2 and 9×10^{14} cm^{-3} O_2, our maximum laser fluence generated ca. 1.6×10^{12} cm^{-3} C_2H, and over the lifetime of C_2H the concentration of O atoms will increase to 2×10^{11} cm^{-3} at most. A simple simulation of the emission intensities with and without O-atom production from R1 shows a difference of less than 2% in the derived $t = \theta$ intensity values when $k_{2b}/k_{1e} = 1000$ is adopted. This is about the maximum deviation expected under all of our experimental conditions. O-atom production from the photolysis of O_2 at 193 nm is entirely negligible.[42]

At room temperature the spectra of the CH(A,B→X) emissions resulting from both the $C_2H + O_2$ and the $C_2H + O(^3P)$ reactions, were also recorded in the presence of 10 Torr He. For the latter reaction, SO_2 was used as a photolytic precursor for O(^{3}P) atoms. The spectra were constructed by replacing the 430 nm interference filter with a high-throughput monochromator (Minichrom PCM-01, Optimetrics) operated with a spectral resolution of 1 nm. Following CH(A,B) production, a portion of the observed time-resolved emission signal, from 10 to 50 μs, was integrated using a boxcar integrator (SR250, Stanford Research Systems). The resulting integrated voltage was passed to a 16-bit analogue-to-digital converter and stored as a single spectral data point on computer. Again, data points were collected at a frequency of 8 Hertz. Several wavelength scans of the monochromator were made and averaged to construct the final emission spectra.

To observe at least some of the initial CH(A,B) rotational distributions for these reactions, particularly to establish whether reactions R1 and R2 differ markedly in this respect, N_2 was replaced by He as the buffer gas, for the spectral scans. It was not attempted to record nascent CH(A,B) rotational distributions as the very low pressures required would allow potential interference from nonthermalized C_2H in the yields of excited CH from the reactions with O_2 and O.

Results and Discussion

Figure 1 shows examples of a series of emission decay profiles, Iem$_t$, at various temperatures, but collected under conditions of identical flow rates of O_2, C_2H_2, and N_2, and at the same total pressure of 10 Torr, such that both [C_2H_2] and [O_2] scale simply as T^{-1}. Least-squares fitting to these averaged emission profiles yields relative values of Iem$_{t=\theta}$ and an absolute decay constant, k' ($k' = k_1[O_2] + k_{12}[C_2H_2]$). The decay constants for these profiles are all in close agreement with those expected on the basis of the literature $k_1(T)$ expression[43] of $3.15 \times 10^{-11}(T/298)^{-0.16}$ cm^3 s^{-1} and a temperature-independent rate constant for k_{12} of 1.5×10^{-10} cm^3 s^{-1}.[38,39]

One must consider the possibility of the relative C_2H yield from photodissociation of C_2H_2 at 193 nm changing with temperature. Contrary to earlier suggestions, it has recently been established that the 193 nm C_2H_2 photolysis occurs solely by a direct process, with an H + C_2H quantum yield of 1.0.[44] The absorption cross-section of C_2H_2, $\sigma(C_2H_2)$, at 193 nm would only change significantly with temperature if the absorption originated, wholly or partially, from an excited vibrational level of C_2H_2. However, a detailed study of the temperature dependence of the absolute absorption cross-section of C_2H_2 showed the absorption region below 197 nm to be due solely to a "cold" band and to be independent of temperature.[45] We therefore expect any changes in absorption cross-section of C_2H_2 at 193 nm and quantum yield for C_2H production to be negligible in our experiments. This is in contrast to species often used as photolytic sources of O-atoms, such as SO_2, N_2O, and NO_2, which have temperature-dependent absorption cross-sections. For this reason it is difficult to derive the temperature dependence of the rate constant for $C_2H + O(^3P) \rightarrow CH(A) + CO$ by the same method as used here for R1e.

To calculate the effects of quenching of CH(A) by N_2, and thus determine the parameter $Q(T)$ of eqs vi and vii, we directly measured the lifetime of CH(A) under typical experimental conditions at several elevated temperatures. For these measurements CH(A) was produced by two-photon photolysis at 193 nm of $2.6 \times 10^{14}(295\text{ K}/T)$ cm^{-3} C_2H_2 in the presence of 10 Torr N_2 and the resulting CH(A) emission followed as a function of time using a fast digital oscilloscope. The highest-temperature lifetime measurements and those at 295 K were also performed in the presence of 10 Torr He. These results are plotted in Figure

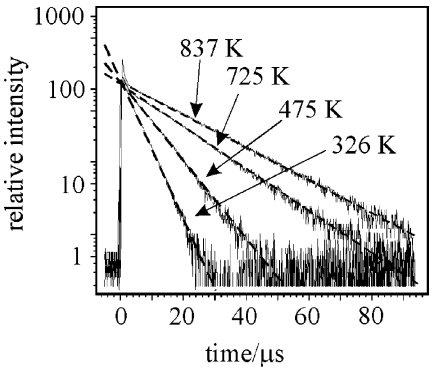

Figure 1. 431 nm CH(A→X) emission profiles arising from CH(A) produced in the $C_2H + O_2$ reaction following 193 nm photoproduction of C_2H from C_2H_2 in the presence of O_2. Conditions: [C_2H_2] = $3.9 \times 10^{14}(326/T)$, [$O_2$] = $5.6 \times 10^{15}(326/T)$, and total pressure of 10 Torr N_2. Dashed lines are least-squares fits used to obtain relative intensities at zero time for the various T. The change in decay constants with temperature reflects the slower removal of C_2H due mainly to the changes in density of O_2 and C_2H_2.

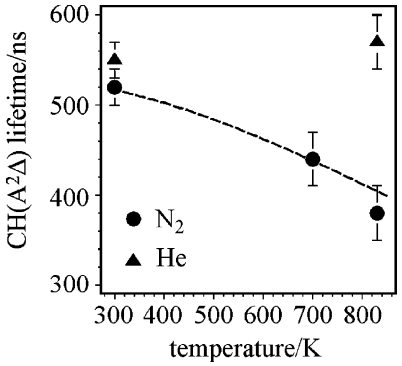

Figure 2. Results of CH($A^2\Delta$) lifetime measurements following production of CH(A) by two-photon dissociation of C_2H_2 at 193 nm. Circles: (1/e) lifetime of CH(A) in the presence of 10 Torr N_2. Triangles: CH(A) lifetime in the presence of 10 Torr He. The concentration of C_2H_2 in each case was $1 \times 10^{15} \times (295/T)$ cm^3. The dotted line represents the predicted lifetime of CH(A) in the presence on 10 Torr N_2 based on the N_2 quenching cross-section data given by Tamura et al.[37]

TABLE 1: Results of Determinations of Intercepts at $t = \theta$ of Time-Resolved $[CH(A)]_{ss}$ Emission Profiles Arising from the $C_2H + O_2 \rightarrow CH(A) + CO_2$ Reaction under Three Sets of Reaction Conditions

data set 1[a]			data set 2[b]			data set 3[c]					
T	I^d	k_r^e	T	I^d	k_r^e	T	I^d	k_r^e	$G \times T^f$	$Q(T)^g$	$\Phi(T_{ref})/\Phi(T)^h$
326	1.000	1.00	320	1.000	1.00	316	1.000	1.00	1.00	1.00	1.000
395	0.817	1.19	387	0.831	1.22	357	0.919	1.19	1.18	1.01	1.010
475	0.754	1.60	466	0.823	1.75	466	0.750	1.66	1.62	1.05	1.031
555	0.714	2.06	547	0.805	2.35	547	0.739	2.24	2.19	1.09	1.053
641	0.707	2.74	635	0.824	3.25	635	0.692	2.88	2.75	1.14	1.059
725	0.728	3.60	715	0.845	4.23	715	0.705	3.66	3.55	1.19	1.075
784	0.767	4.44	787	0.884	5.35	787	0.738	4.65	4.49	1.24	1.087
837	0.828	5.46	837	0.945	6.47	839	0.783	5.59	5.42	1.27	1.099

[a] Data set 1: $[C_2H_2] = 3.9 \times 10^{14}$ (326 K/T) cm^3, $[O_2] = 5.6 \times 10^{15}$ (326 K/T). [b] Data set 2: $[C_2H_2] = 6.9 \times 10^{14}$ (320 K/T) cm^3, $[O_2] = 1.9 \times 10^{15}$ (320 K/T) cm^3. [c] Data set 3: $[C_2H_2] = 1.4 \times 10^{15}$ (316 K/T) cm^3, $[O_2] = 5.5 \times 10^{14}$ (316 K/T) cm^3. [d] Relative CH(A→X) emission intensity at $t = \theta$, $Iem_{t=\theta}(T)/Iem_{t=\theta}(T_{ref})$ where T_{ref} is 326, 320, and 316 K for data sets 1, 2, and 3, respectively. [e] $k_r = I(T/T_{ref})^2$ where T_{ref} is 326, 320, and 316 K for data sets 1, 2, and 3, respectively. [f] Integrated detected emission intensity, G, multiplied by temperature, relative to 316 K values. [g] Values of $Q(T)$ are relative to that at the reference temperature of 320 K and apply to all data sets. [h] $\Phi(T_{ref})/\Phi(T)$: the optical transmission of the interference filter for CH(A) having rotational temperature T, relative to that at 320 K. The various temperatures at which $\Phi(T)$ is calculated are 320, 370, 470, 550, 638, 720, 785, and 837 K.

2. As can be seen, there is a clear effect of temperature on the lifetime of CH(A) in the presence of 10 Torr N_2, whereas for He hardly any change is noticeable between 295 and 830 K. Our measurements for N_2 agree closely with that predicted using the quenching cross-section data given by Tamura et al.[37] We therefore chose to use directly the data from this reference to calculate $Q(T)$ for our $Iem_{t=\theta}$ determinations. Note that the value of θ changes from 520 ns at 320 K to 400 ns at 830 K.

In total, three separate sets of experiments were carried out covering $[C_2H_2]/[O_2]$ ratios from 0.07 to 2.54. For the last data set, with $[C_2H_2]/[O_2] = 2.54$, an integrated intensity analysis was also done.

Table 1 summarizes, for each set of data, the three determined components of eq iv used to derive $k_{1e}(T)/k_{1e}(T_{ref})$. These are k_r $\{=Iem_{t=\phi}(T)/Iem_{t=\phi}(T_{ref}) \times (T/T_{ref})^2\}$ derived from the intercepts of the $[CH(A)]_{ss}$ profiles, the first correction term, $Q(T)$, describing the effects of quenching of CH(A) by N_2, and the second correction term, $\Phi(T_{ref})/\Phi(T)$, describing the effective total change in transmission of the CH(A→X) $\Delta\nu = 0$ transition through the interference filter at various temperatures. For data set 3, the integrated intensity values (denoted by G) multiplied by T are also given.

Values of $k_rQ(T)\{\Phi(T_{ref})/\Phi(T)\}$ $(=k_{1e}(T)/k_{1e}(T_{ref}))$ from Table 1, together with values of $Q(T)$ $G(T)T$ $\{\Phi(T_{ref})/\Phi(T)\}$ $(=k_{1e}(T)/k_{12}(T) \times k_{12}(T_{ref})/k_{1e}(T_{ref}))$ from data set 3 of Table 1 are plotted in Figure 3 after all being scaled by a factor 1.1 so that the fitted function (given below) equals 1.0 at 300 K. The expected relative systematic uncertainty between the 316 K determinations and the 837 K determinations of $k_{1e}(T)/k_{12}(T)$ using the integrated intensities, with the approximation that $k_{12}[C_2H_2] \gg k_2[O_2]$, is about 5% under conditions of data set 3. Values of $Q(T)$ $G(T)T\{\Phi(T_{ref})/\Phi(T)\}$ are plotted as small filled circles in Figure 3. The other sets of data are grouped for analysis and a function of the form $AT^n \exp(B/T)$ is fitted to them using the weighted least-squares procedure. The fit yields a temperature dependence of k_{1e} over the temperature range 316−837 K of $k_{1e}(T)/k_{1e}(T_{ref}) = AT^{4.4} \exp[(1150 \pm 150 \text{ K})/T]$, where A is a constant and the (2σ) uncertainty over the experimental temperature range is best expressed by the uncertainty in the argument of the exponential function. If we extrapolate this expression to higher temperatures, we predict a factor 15 ± 4, 60 ± 16, and 190 ± 45 increase in k_{1e} from 300 to 1000, 1500, and 2000 K, respectively.

There is some earlier indirect evidence that k_{1e} increases strongly with temperature: Matsuda et al.[21] estimated an activation energy for this reaction of 105 kJ mol^{-1} from the temperature dependence of CH(A) emission signals in shock tubes over the range $T = 1100-2400$ K. When this activation energy was used by Hwang et al.[46] in a modeling study, the model agreed qualitatively with the available (shock-tube) experimental data of CH(A→X) emission intensities, though these authors did not consider reaction k_{2b} in the kinetic model and, at that time, knowledge of formation routes for C_2H were sketchy. Over this same temperature range our results would reproduce an apparent activation energy of only 50 kJ mol^{-1}.

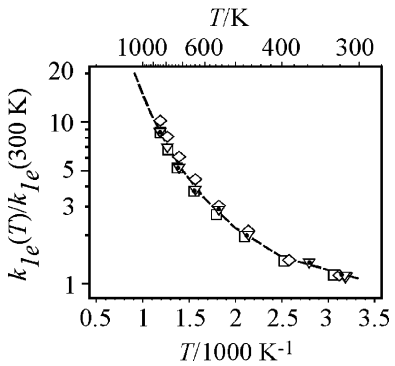

Figure 3. Relative increase in rate constant k_{1e} as a function of temperature. The data points represent $t = \theta$ values of emission intensities at 431 nm such as those given in Figure 1. Each emission intensity is corrected for the change in gas density (hence $[O_2]$ and $[C_2H_2]$) as a function of temperature (eq v) and quenching by N_2. The C_2H_2 and O_2 concentrations were as follows: squares (data set 1) $[C_2H_2] = 3.9 \times 10^{14}$(326 K/$T$) cm^3, $[O_2] = 5.6 \times 10^{15}$(326 K/$T$) cm^3; diamonds (data set 2) $[C_2H_2] = 6.9 \times 10^{14}$(320 K/$T$) cm^3, $[O_2] = 1.9 \times 10^{15}$(320 K/$T$) cm^3; triangles (data set 3) $[C_2H_2] = 1.4 \times 10^{15}$(316 K/$T$) cm^3, $[O_2] = 5.5 \times 10^{14}$(316 K/$T$) cm^3. The pressure was 10 Torr (N_2) for all experiments. For comparison, the small filled circles represent the integrated intensity of each decay for data set 3, corrected for the change in density with temperature of $[O_2]$ (eqn. vi) and quenching by N_2. The line represents a least-squares $AT^n \exp(B/T)$ fit to the combined data sets, (i.e. excluding the integrated intensity values). The best fit gives $B = 1150 \pm 150$ and $n = 4.4$.

To put these findings for k_{1e} in context for hydrocarbon flames requires a comparison with the competitive chemiluminescence reaction k_{2b}. For this reason, as described in the Experimental Section, spectral scans of the time-resolved emissions for reactions R1e and R2b were performed to ascertain if there were any obvious differences in the CH(A,B) nascent vibrational, rotational, and A/B electronic populations. Figure 4 shows the CH(A→X) spectra arising from reaction R1e and reaction R2b together with a simulation (dotted line).[47] The CH(A→X) spectrum arising from reaction R1e, shifted above the baseline

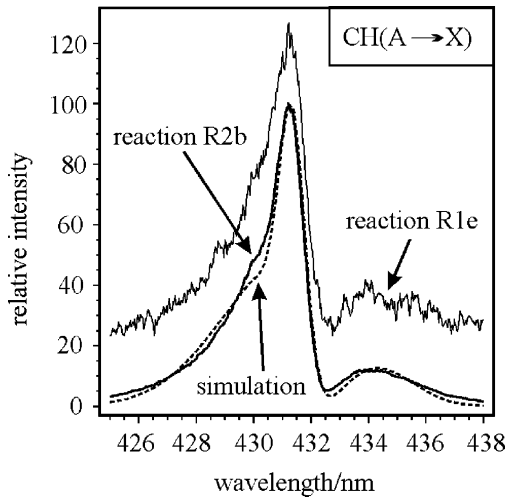

Figure 4. CH(A−X) emission spectra at 1 nm resolution arising from CH(A) formed in reaction R1e (upper line, baseline-shifted for clarity) and R2b (bottom solid line) at 295 K. The dotted line is a simulated spectra with CH(A) possessing a statistical rotation distribution of 600 K. The difference in shape between the simulation and the experimental spectra is indicative of partial rotational relaxation by 10 Torr He from a higher-temperature rotational distribution.

for clarity, follows very closely that arising from reaction R2b. The shape of the simulation spectra in this spectral region and at 1 nm resolution is not very sensitive to the vibrational population distribution, which could therefore not be ascertained. The best fit simulation for CH(A) from both R1e and R2b is that for a rotational temperature of 600 K. However, there are distinct differences in the shape of the R- and P-branchenvelopes between the simulation and the experimental spectra. Similar differences are also present in the CH(A→X) spectra observed in low-pressure C_2H_2/O/H atomic flames.[48] These differences might be attributed to partial quenching by He of the CH(A) rotational levels during its average radiative lifetime of 540 ns. For the rotational levels significantly populated here, the rate constant for rotational quenching ($\Delta N = -1$) by He[49] ranges from ca. 3×10^{-11} cm^3 s^{-1} for $N = 11$ to ca. 1.4×10^{-10} cm^3 s^{-1} for $N = 4$ such that for 10 Torr He partial quenching occurs with ($\Delta N = -1$) quenching from levels $N = 4$ to $N = 9$, being more rapid than for levels $N > 9$. This would result in an initial statistical rotational distribution (above room temperature) having rotational populations shifted from the midrotational levels ($N = 4-9$) to the lower ones ($N > 4$) with less depopulation observed for levels with $N > 9$. Taking a quenching rate constant of 1×10^{-10} cm^3 s^{-1}, the rate of quenching of rotational levels in 10 Torr He would be of the order of 3×10^6 s^{-1}; this, when compared to the removal rate by spontaneous emission of ca. 2×10^6 s^{-1}, supports our interpretation of partial rotational quenching. We therefore expect an initial rotational distribution, if statistical, to be above 600 K for this reaction occurring at room temperature.

CH(A→X) and CH(B→X) transitions were observed for both reaction R1e and R2b. The ratio CH(A)/CH(B) was estimated to be about 20 at 295 K for R2b after corrections applied on the basis of supplied wavelength responsivity data for the monochromator and for our PMT. In fact, the relative A-to-B populations for the two reactions studied are quite similar at room temperature, with

$$\frac{\text{R2b}\{[\text{CH(A)}]/[\text{CH(B)}]\}}{\text{R1e}\{[\text{CH(A)}]/[\text{CH(B)}]\}} = 0.8 \pm 0.2$$

Note that this value is independent of the wavelength responsivity of our system.

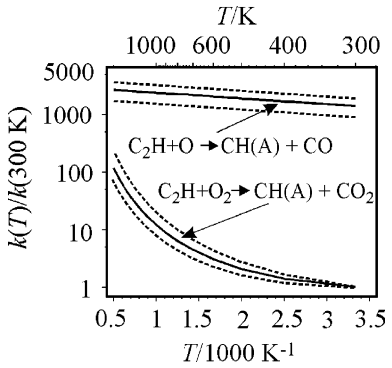

Figure 5. Best fit lines representing the rate constants $k_{1e}(T)$ (lower solid line) and $k_{2b}(T)$ (upper solid line) relative to k_{1e}(300 K). The T dependence for k_{1e} is derived from the present study, and that of k_{2b} is from ref 28. The dashed lines represent 95% confidence limits for random uncertainites. The ratio of the rate constants k_{2b}(300 K)/k_{1e}(300 K) is derived from the present study: our estimated systematic uncertainty in this value is ±500.

At 295 K we also determined the ratios of rate constant k_{2b}/k_{1e} via two different methods. The first was similar to that employed earlier by Devriendt et al.[28] by comparing the $\text{Iem}_{t=\theta}$ signals when O_2 is replaced by an O-atom photolytic precursor. Here we used N_2O and a 193 nm absorption cross-section of 1.0×10^{-19} cm^2 and a quantum yield of unity for O(^{3}P) production following rapid quenching of O(^{1}D) by N_2.[50,51] Under these conditions we derived a ratio k_{2b}(295 K)/k_{1e}(295 K) of 1400 with an estimated systematic error of ±500. Our second determination of the same ratio was done by comparing the intensities of the spectra in Figure 3. Here SO_2 was used as the O-atom precursor having an absorption cross-section of 6×10^{-18} cm^2 at 193 nm.[52] When corrections are made for differences in removal rates over the signal integration time 10−50 μs, we arrive at k_{2b}(295 K)/k_{1e}(295 K) = 1000, with an estimated systematic error similar to the first determination using N_2O. By combining our k_{2b}/k_{1e} ratio at room temperature with the activation energy of R2b derived by Devriendt et al.,[28] we are able to compare k_{1e} and k_{2b} as a function of temperature. This is shown in Figure 5. As can be seen k_{1e} increases much more rapidly with temperature than does k_{2b}, with the result that the ratio is predicted to change from ca. 1200 at room temperature to ca. 40 at 1500 K. Using this last result, the full expression for the absolute rate constant for k_{1e} is best given as $k_{1e}(T) = 1 \times 10^{-27} T^{4.4} \exp[(1150 \pm 150)\text{ K}/T]$. Though the T dependence for reaction R1e is well characterized in the present study, the absolute rate constant at any given temperature between 300 K and ca. 1000 K is expected to be known to only within an order of magnitude.

Conclusions

We have determined the temperature dependence of the rate constant, k_{1e}, for the $C_2H + O_2 \rightarrow CH(A) + CO_2$ reaction over the temperature range 316−837 K. The results show an increase in k_{1e} of a factor ca. 8 ± 1 over this temperature range, and we predict an increase of a factor 60 ± 16 between 300 and 1500 K. This large increase in rate constant compared to the less pronounced increase in the rate constant of the competitive chemiluminescence reaction $C_2H + O(^3P) \rightarrow CH(A) + CO$ implies that the former reaction will have a much greater contribution to CH(A) formation in hydrocarbon flames than is presently assumed. Reaction R1e may dominate CH(A) production in flames with equivalence ratios less than unity, in which the $[O_2]/[O]$ ratio is more than about 50 ± 30. Spectroscopic measurements in flames might be able to discern

a difference between CH(A→X) to CH(B→X) intensity ratios under fuel-rich and fuel-lean conditions. A difference should be indicative of the dominance of reaction R2b under fuel-rich conditions and R1e under fuel-lean conditions.

Acknowledgment. We thank Professor J. Peeters for helpful discussion on this project. We are also indebted to the Flemish Fund for Scientific Research, FWO-Vlaanderen (postdoctoral fellowship, research project), and the KULeuven Research Council (GOA program, doctoral scholarship) for continuing financial support.

References and Notes

(1) Grebe, J.; Homann, K. H. *Ber. Bunsen-Ges. Phys. Chem.* **1981**, *86*, 588 and references therein.
(2) Becker, K. H.; Heinemeyer, F.; Horie, O. *Ber. Bunsen-Ges. Phys. Chem*. **1983**, *87*, 898 and references therein.
(3) Dandy, S. D.; Vosen, S. R. *Combust. Sci. Technol*. **1992**, *82*, 131 and references therein.
(4) Fontijn, A.; Goumri, A.; Brock, P. E. *Combust. Flame* **2000**, *121*, 699 and references therein.
(5) Burke, M. L.; Dimpfl, W. L.; Sheaffer, P. M.; Zittel, P. F.; Bernstein, L. S. *J. Phys. Chem.* **1996**, *100*, 138 and references therein.
(6) Staicu, A.; Stolk, R. L.; Meulen, J. J. *J. Appl. Phys.* **2002**, *91*, 969 and references therein.
(7) Grebe, J.; Homann, K. H. *Ber. Bunsen-Ges. Phys. Chem.* **1981**, *86*, 581.
(8) Fontijn, A.; Johnson, S. E. *J. Chem. Phys.* **1973**, *59*, 6193.
(9) Dandy, D. S.; Vosen, S. R. *Combust. Sci. Technol*. **1992**, *82*, 131.
(10) Hardalupas, Y.; Orain, M.; Panoutsos, C. S.; Taylor, A. M. K. P.; Olofsson, J.; Seyfried, H.; Richter, M.; Hult, J.; Ald, M.; Hermann, F.; Klingmann, J. *Appl. Therm. Eng.* **2004**, *24*, 1619.
(11) Higgins, B.; McQuay, M. Q.; Lacas, F.; Rolon, J. C.; Darahiba, N.; Candel, S. *Fuel* **2001**, *80*, 67.
(12) Higgins, B.; McQuay, M. Q.; Lacas, F.; Candel, S. *Fuel* **2001**, *80*, 1583.
(13) Docquier, N.; Lacas, F.; Candel, S. *Proc. Combust. Inst.* **2002**, *29*, 139.
(14) Najm, H. N.; Paul, P. H.; Mueller, C. J.; Wycoff, P. S. *Combust. Flame* **1998**, *113*, 312.
(15) Hardalupas, Y.; Orain, M. *Combust. Flame* **2004**, *139*, 188.
(16) Walsh, K. T.; Long, M. B.; Tanoff, M. A.; Smooke, M. D. *Proc. Combust. Inst***. 1998**, *27*, 615.
(17) Luque, J.; Jeffries, J. B.; Smith, G. P.; Crosley, D. R.; Walsh, K. T.; Long, M. B.; Smooke, M. D. *Combust. Flame* **2000**, *122*, 172.
(18) Glass, G. P.; Kistiakowsky, G. B.; Michael, J. V.; Niki, H. *Proc. Combust. Inst.* **1965**, *10*, 513.
(19) Gaydon, A. G. *The Spectroscopy of Flames*; Wiley: New York, 1957; pp 160 and 197.
(20) Porter, R. P.; Clark, A. H.; Kastkan, W. E.; Browne, W. E. *Proc. Combust. Inst*. **1967**, *11*, 907.
(21) Matsuda, S.; Slagle, I. R.; Fife, D. F.; Marquart, J. R.; Gutman, D. *J. Chem. Phys.* **1972**, *57*, 5277.
(22) Renlund, A. M.; Shoohi, F.; Reisler, H.; Wittig, C. *Chem. Phys. Lett.* **1981**, *84*, 293.
(23) Peeters, J.; Boullart, W.; Langhans, I. *Int. J. Chem. Kinet*. **1994**, *26*, 869.
(24) Peeters, J.; Boullart, W.; Devriendt K. *J. Phys. Chem*. **1995**, *99*, 3583.
(25) Boullart, W.; Devriendt, K.; Borms, R.; Peeters, J. *J. Phys. Chem.* **1996**, *100*, 998.
(26) Ollivier, J. L.; Dobrijévic, M.; Parisot, J. P. *Planetary Space Sci.* **2000**, *48*, 699 and references therein.
(27) Devriendt, K.; Peeters, J. *J. Phys. Chem. A* **1997**, *101*, 2546.
(28) Devriendt, K.; Van Look, H.; Ceursters, B.; Peeters, J. *Chem. Phys. Lett*. **1996**, *261*, 450. A rate constant for k_{2b} at 298 K was determined in that study of $k_{2b} = (1.8 \pm 0.7) \times 10^{-11}$ cm^3 s^{-1}. That value was based on a quantum yield for C_2H production from C_2H_2 photodissociation at 193 nm of 0.25. However, recent publications [Lauter, A.; Lee, K. S.; Jung, K. H.; Vatsa, R. K.; Mittal, J. P.; Volpp, H. R. *Chem. Phys. Lett*. **2002**, *358*, 314. Shokoohi, F.; Watson, T. A.; Reisler, H.; Kong, F.; Renlund, A. M.; Wittig, C. *J. Phys. Chem*. **1986**, *90*, 5695] show that this quantum yield is about unity. Using this new value, the originally quoted value of k_{2b}(295 K) should be revised to 4.5×10^{-12} cm^3 s^{-1}. This value, in combination with the activation energy derived in the study of ref 27, gives our preferred Arrhenius expression for this rate constant of $k_{2b}(T) = (1.0 \pm 0.5) \times 10^{-11}$ exp(−230/T(K)) cm^3 s^{-1}.
(29) Chikan, V.; Nizamov, B.; Leone, S. R. *J. Phys. Chem.* **2004**, *108*, 10770.
(30) Van Look, H.; Peeters, J. *J. Phys. Chem*. **1995**, *99*, 16284.
(31) Nizamov, B.; Leone, S. R. *J. Phys. Chem. A* **2004**, *108*, 1746 and references therein.
(32) Carl, S. A.; Nguyen, H. M. T.; Elsamra R. M. I.; Nguyen, M. T.; Peeters, J. *J. Chem. Phys.* **2005**, *122*, 114307 and references therein.
(33) Carl, S. A.; Nguyen, H. M. T.; Nguyen, M. T.; Peeters, J. *J. Chem. Phys.* **2003**, *118*, 10996.
(34) Smith, G. P.; Luque, J.; Park, C.; Jeffries, J. B.; Crosley, D. R. *Combust. Flame* **2002**, *131*, 59.
(35) Vértesi, T.; Bene, E.; Vibók, A.; Halász, G. J.; Baer, M. *J. Phys. Chem. A* **2005**, *109*, 3476.
(36) Luque, J.; Crosley, D. R. *J. Chem. Phys*. **1996**, *104*, 2146.
(37) Tamura, M.; Berg, P. A.; Harrington, J. E.; Luque, J.; Jeffries, J. B.; Smith, G. P.; Crosley, D. R. *Combust. Flame* **1998**, *114*, 502.
(38) Ceursters, B.; Nguyen, H. M. T.; Peeters, J.; Nguyen, M. T. *Chem. Phys.* **2000**, *262*, 243.
(39) A summary of recent determinations of k_{12} and k_2 is given by: Vakhtin, A. B.; Heard, D. E.; Smith, I. W. M.; Leone, S. R. *Chem. Phys. Lett*. **2001**, *344*, 317.
(40) Sumathi, R.; Peeters, J.; Nguyen, M. T. *Chem. Phys. Lett*. **1998**, *287*, 109.
(41) Bai, H. T.; Huang X. B.; Yu, J. K.; Sun, J. Z. *Acta Chim. Sinica* **2004**, *62*, 461.
(42) Yoshino, K.; Esmond, J. R.; Cheung, A. S.-C.; Freeman, D. E.; Parkinson, W. H. *Planet. Space Sci*. **1992**, *40*, 185.
(43) Thiesemann, H.; Taatjes, C. A. *Chem. Phys. Lett*. **1997**, *270*, 580.
(44) Lauter, A.; Lee, K. S.; Jung, K. H.; Vatsa, K. R.; Mittal, J. P.; Volpp, H. R. *Chem. Phys. Lett*. **2002**, *358*, 314.
(45) BeÂnilan, Y.; Smith, N.; Jolly, A.; Raulin, F. *Planet. Space Sci.* **2000**, *48*, 463.
(46) Hwang, S. M.; Gardinger, W. C., Jr.; Frenklach, M. *Combust. Flame* **1987**, *67*, 65.
(47) Luque J.; Crosley, D. R., LIFBASE version 1.6 1st ed., SRI International, MP-99-0099, www.sri.com/cem/lifbase, 1999.
(48) K. Derviendt, Ph.D. Thesis, KULeuven, 1997, p 159 (unpublished).
(49) Wang, C.-C.; Chen, Y.-P.; Chin, T.-L.; Huang, H.-Y.; Lin, K.-C. *J. Chem. Phys.* **2000**, *112*, 10204.
(50) Selwyn, G. S.; Johnston, H. S. *J. Chem. Phys*. **1981**, *74*, 3791.
(51) Nishida, S.; Takahashi, K.; Matsumi, Y.; Taniguchi, N.; Hayashida, S. *J. Phys. Chem. A* **2004**, *108*, 2451.
(52) Manatt, S. L.; Lane A. L. *J. Quant. Spectrosc. Radiat. Transfer* **1993**, *50*, 267 and references therein.